Phenomenological thermodynamic potential for CaTiO₃ single crystals

Yijia Gu,[1,*] Karin Rabe,[2] Eric Bousquet,[3,4] Venkatraman Gopalan,[1] and Long-Qing Chen[1]

[1]*Department of Materials Science and Engineering, Pennsylvania State University, University Park, Pennsylvania 16802, USA*
[2]*Department of Physics and Astronomy, Rutgers University, Piscataway, New Jersey 08854-8019, USA*
[3]*Department of Materials, ETH Zürich, Wolfgang-Pauli-Strasse 27, CH-8093 Zürich, Switzerland*
[4]*Physique Théorique des Matériaux, Université de Liège, B-4000 Sart Tilman, Belgium*

The antiferrodistortive (AFD) structural transitions of calcium titanate (CaTiO₃) at ambient pressure have been extensively studied during the last few years. It has been found that none of the AFD polymorphs is polar or ferroelectric. However, it was recently shown theoretically and later experimentally confirmed that a ferroelectric transition in CaTiO₃ can be induced by tensile strains. The ferroelectric instability is believed to be strongly coupled to the AFD soft modes. In this paper, we present a complete thermodynamic potential for describing the coupling between the AFD and ferroelectric phase transitions. We analyzed the dependence of transition temperatures on stress and strain condition. Based on this potential, a (001) CaTiO₃ thin film diagram was constructed. The results show good agreement with available experimental observations. The strong suppression of ferroelectric transition by the AFD transition is discussed.

I. INTRODUCTION

The ideal perovskite structure, described as a simple cubic network of corner linked BO_6 octahedra with A atoms occupying 12-fold oxygen coordinated sites, is inherently unstable and can exhibit a variety of distortions. These include polar distortions, dominated by off-centering of the B cation in its oxygen octahedron, and tilts and rotations of the oxygen octahedron network. The polar distortions lead to the presence of dipoles and to ferroelectric and antiferroelectric behavior in several well-known perovskite compounds, such as BaTiO₃, PbTiO₃, PbZrO₃, and BiFeO₃.[1] Oxygen octahedron rotations produce a variety of nonpolar phases, the phase transitions of which are called antiferrodistortive (AFD) phase transitions. The same compound can show instabilities to both distortions in the cubic phase, in which case they usually compete. Strontium titanate (SrTiO₃) is a good example of such compounds. Although SrTiO₃ has a ferroelectric instability, it is paraelectric all the way down to 0 K. Its ferroelectric transition is weakened along the direction of AFD tilt.[2,3] With a sufficiently large epitaxial strain, SrTiO₃ becomes ferroelectric even at room temperature.[4]

At ambient temperature and pressure, calcium titanate (CaTiO₃) has the orthorhombic distorted-perovskite structure with space group *Pbnm*, a structure common to many perovskite oxides. Disregarding the distortion of TiO₆ octahedra, the structure of CaTiO₃ can be illustrated as a combination of two kinds of TiO₆ octahedron tilts: two out-of-phase tilts along x_1 and x_2 directions, and one in-phase tilt along x_3 direction (Fig. 1). With the standard Glazer's notation,[5] it can be expressed as $a^- a^- c^+$. These two kinds of tilts can also be used to characterize the AFD transitions in CaTiO₃. We will discuss it in more details later.

The AFD transition sequence of CaTiO₃ is complicated. From high to low temperature, CaTiO₃ transforms from cubic ($Pm\bar{3}m$) to tetragonal ($I4/mcm$) at about 1600 K, and from tetragonal ($I4/mcm$) to orthorhombic at about 1500 K.[6–11] The later transition or transitions is quite controversial. Ali and Yashima[10,11] proposed a direction transition from $I4/mcm$

to *Pbnm* by the Rietveld analysis of high-temperature x-ray and neutron diffraction data. Also by the analysis of high-temperature neutron diffraction data, Kennedy *et al.*[9] found there might be an intermediate phase with *Cmcm* structure between the transition from $I4/mcm$ to *Pbnm*. And the transition temperature from *Cmcm* to *Pbnm* is around 1380 K, which agrees with both the drop-calorimetry measurements of Guyot *et al.*[7] and the Raman spectroscopy observation of Gillet *et al.*[12] On the other hand, Carpenter theoretically investigated the structural transitions of CaTiO₃ using Landau theory, and he concluded that in order to get a stable *Pbnm* structure, there must be some intermediate structure between $I4/mcm$ and *Pbnm*. However, he proposed an $I4/mcm \rightarrow Imma \rightarrow Pbnm$ transition sequence.

Despite of the complicity and discrepancy, none of the above-mentioned structures is polar or ferroelectric at ambient pressure. However, CaTiO₃ has a ferroelectric soft mode as manifested by a high dielectric constant at low temperature[13] and later first-principles calculations.[14] Experiments also show frequency independence of CaTiO₃ dielectric constants, which makes it a high-quality microwave material. Therefore, similar to SrTiO₃, CaTiO₃ is also an incipient ferroelectric,[13] and the extrapolated ferroelectric transition temperature is about −111 K.[13,15] It is natural to consider the ferroelectricity of CaTiO₃ as an analog to that of SrTiO₃, which is weakened by AFD, but can be induced by applied strain.[2–4,16] In addition, some other perovskites with *Pbnm* structures, including CaMnO₃,[17] SrZrO₃,[18] etc.,[19] are possible to exhibit strain-induced ferroelectricity. Recently, by first-principles calculations, Eklund *et al.*[20,21] predicted that 1.5% epitaxial tensile strain can indeed lead to ferroelectric transition. Experimentally, Vlahos[22] found spontaneous polarization in the CaTiO₃/NdGaO₃ film system with a tensile constraint strain of 1.15%. Thus, ferroelectricity in CaTiO₃ can be induced by a sufficiently large tensile strain.

In addition to the strain-induced ferroelectric behavior of thin films, the twin walls of CaTiO₃ have been extensively investigated, including trapping of oxygen vacancies,[23,24] the
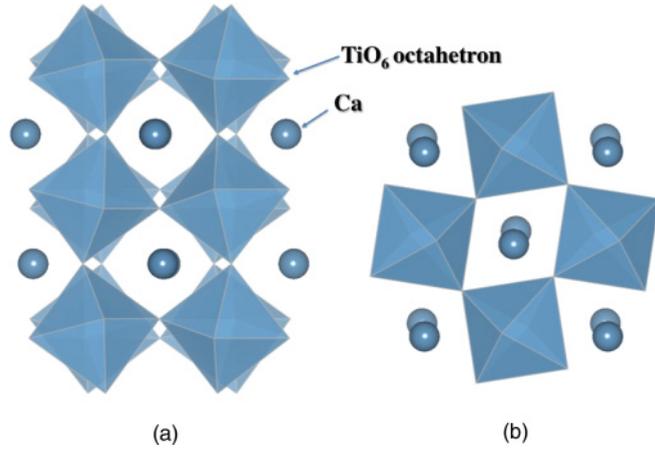
FIG. 1. (Color online) Crystal structure of CaTiO$_3$: (a) projection along [100] direction, the TiO$_6$ octahedra in consecutive two layers exhibit out-of-phase tilt, (the projection along [010] direction is similar); (b) projection along [001] direction, the TiO$_6$ octahedra show in-phase tilt.

activation energy for twin-wall motion,[25] and the intrinsic elasticity of the twin walls.[26] By theoretical simulations, Goncalves-Ferreira *et al.*[27] showed that the CaTiO$_3$ ferroelastic twin walls exhibit sizeable spontaneous polarization due to the vanishing of octahedra tilt and the decrease of the material density. Further experiments show that the twins of CaTiO$_3$ are ferroelectric themselves.[22] Since the formation of twins is usually to lower the total strain energy, the twins themselves are usually strained. Therefore, the discovered ferroelectricity of CaTiO$_3$ twin domains may also be due to strain effect.

In order to control and manipulate its properties with an applied external strain, it is necessary to understand the thermodynamics of CaTiO$_3$. Carpenter *et al.*[28,29] proposed a Landau expansion to describe the AFD transitions in (Ca, Sr)TiO$_3$. Although he made a systematic analysis of the stability of all the possible structures, the ferroelectric transition is not considered, and coefficients were not determined. In this paper, we construct a phenomenological thermodynamic potential for a CaTiO$_3$ single crystal, which incorporates both the AFD transitions and the ferroelectric transitions with different stress and strain conditions. This potential can therefore be employed to analyze all the important phase transitions and their dependence on stress and strain conditions. In the following section, we'll introduce the phenomenological model and convert all the parameters determined from first-principles calculations to this model. In the third section, all the temperature-dependent coefficients will be determined, and some of the parameters from first-principles calculations will be revised from fitting the experimental data. Finally, we'll use a dielectric constant to validate our model and then investigate the competition mechanism of AFD and ferroelectric transitions in the CaTiO$_3$ thin film phase diagram.

II. PHENOMENOLOGICAL DESCRIPTION

The phase transitions in CaTiO$_3$ can be described with a single Landau free energy expansion in terms of ε_i, P_i, and q_i. Here, ε_i ($i = 1$–6) are the strain components following Voigt's convention; P_i ($i = 1, 2, 3$) represent three components of the

spontaneous polarization in the Cartesian coordinate system; and q_i ($i = 1, 2, 3$) represent the linear oxygen displacement that corresponds to simultaneous out-of-phase tilt of TiO$_6$ octahedra. Similarly, q_i ($i = 4, 5, 6$) represent the oxygen displacement of simultaneous in-phase tilt of TiO$_6$ octahedra. The relationship between order parameter q_i and octahedral tilt angles is explained in the Appendix. In terms of soft modes, P_i, q_i ($i = 1, 2, 3$), and q_i ($i = 4, 5, 6$) correspond to the Γ_4^-, R_4^+, M_3^+ modes, respectively. The total free energy has following form:

$$F = F_{\text{Polar}} + F_{\text{OPT}} + F_{\text{IPT}} + F_{\text{Elastic}} + F_{\text{Coupling}}. \quad (1)$$

The first three terms on the right-hand side of Eq. (1) describe contributions from spontaneous polarization, out-of-phase tilt, and in-phase tilt:

$$
\begin{aligned}
F_{\text{Polar}} = {} & \alpha_1(T)\left(P_1^2 + P_2^2 + P_3^2\right) + \alpha_{11}\left(P_1^2 + P_2^2 + P_3^2\right)^2 \\
& + \alpha_{12}\left(P_1^4 + P_2^4 + P_3^4\right) + \alpha_{111}\left(P_1^2 + P_2^2 + P_3^2\right)^3 \\
& + \alpha_{112}\left(P_1^2 + P_2^2 + P_3^2\right)\left(P_1^4 + P_2^4 + P_3^4\right) \\
& + \alpha_{122}(P_1 P_2 P_3)^2,
\end{aligned}
\quad (2)
$$

$$
\begin{aligned}
F_{\text{OPT}} = {} & \beta_1(T)\left(q_1^2 + q_2^2 + q_3^2\right) + \beta_{11}\left(q_1^2 + q_2^2 + q_3^2\right)^2 \\
& + \beta_{12}\left(q_1^4 + q_2^4 + q_3^4\right) + \beta_{111}\left(q_1^2 + q_2^2 + q_3^2\right)^3 \\
& + \beta_{112}\left(q_1^2 + q_2^2 + q_3^2\right)\left(q_1^4 + q_2^4 + q_3^4\right) \\
& + \beta_{122}(q_1 q_2 q_3)^2,
\end{aligned}
\quad (3)
$$

$$
\begin{aligned}
F_{\text{IPT}} = {} & \gamma_1(T)\left(q_4^2 + q_5^2 + q_6^2\right) + \gamma_{11}\left(q_4^2 + q_5^2 + q_6^2\right)^2 \\
& + \gamma_{12}\left(q_4^4 + q_5^4 + q_6^4\right) + \gamma_{111}\left(q_4^2 + q_5^2 + q_6^2\right)^3 \\
& + \gamma_{112}\left(q_4^2 + q_5^2 + q_6^2\right)\left(q_4^4 + q_5^4 + q_6^4\right) \\
& + \gamma_{122}(q_4 q_5 q_6)^2,
\end{aligned}
\quad (4)
$$

where α, β, and γ are constants. Only the coefficients of the second-order terms are assumed to be temperature dependent, i.e.

$$
\begin{aligned}
\alpha_1(T) &= \alpha_{10}\Theta_{S1}\left[\coth\left(\frac{\Theta_{S1}}{T}\right) - \coth\left(\frac{\Theta_{S1}}{T_1}\right)\right], \\
\beta_1(T) &= \beta_{10}\Theta_{S2}\left[\coth\left(\frac{\Theta_{S2}}{T}\right) - \coth\left(\frac{\Theta_{S2}}{T_2}\right)\right], \quad (5) \\
\gamma_1(T) &= \gamma_{10}\Theta_{S3}\left[\coth\left(\frac{\Theta_{S3}}{T}\right) - \coth\left(\frac{\Theta_{S3}}{T_3}\right)\right],
\end{aligned}
$$

where T_1, T_2, and T_3 are Curie temperatures, and Θ_{S1}, Θ_{S2}, and Θ_{S3} are saturation temperatures. The strain contribution to the total free energy can be written as

$$F_{\text{Elastic}} = \tfrac{1}{2}C_{11}\left(\varepsilon_1^2 + \varepsilon_2^2 + \varepsilon_3^2\right) + C_{12}(\varepsilon_1\varepsilon_2 + \varepsilon_3\varepsilon_2 + \varepsilon_1\varepsilon_3) + \tfrac{1}{2}C_{44}\left(\varepsilon_4^2 + \varepsilon_5^2 + \varepsilon_6^2\right), \quad (6)$$

where C_{11}, C_{12}, and C_{44} are elastic stiffness constants, and ε_1–ε_6 are strain components. The coupling energy among

different-order parameters and strains is written as

$$
\begin{aligned}
F_{\text{Coupling}} = &-t_{11}\left(P_1^2 q_1^2 + P_2^2 q_2^2 + P_3^2 q_3^2\right) - t_{12}\left[P_1^2\left(q_2^2 + q_3^2\right) + P_2^2\left(q_1^2 + q_3^2\right) + P_3^2\left(q_1^2 + q_2^2\right)\right] \\
&- t_{44}(P_1 P_2 q_1 q_2 + P_1 P_3 q_1 q_3 + P_2 P_3 q_2 q_3) - \kappa_{11}\left(P_1^2 q_4^2 + P_2^2 q_5^2 + P_3^2 q_6^2\right) \\
&- \kappa_{12}\left[P_1^2\left(q_5^2 + q_6^2\right) + P_2^2\left(q_4^2 + q_6^2\right) + P_3^2\left(q_4^2 + q_5^2\right)\right] - \kappa_{44}(P_1 P_2 q_4 q_5 + P_1 P_3 q_4 q_6 + P_2 P_3 q_5 q_6) \\
&- \mu_{11}\left(q_1^2 q_4^2 + q_2^2 q_5^2 + q_3^2 q_6^2\right) - \mu_{12}\left[\left(q_2^2 + q_3^2\right)q_4^2 + \left(q_3^2 + q_1^2\right)q_5^2 + \left(q_1^2 + q_2^2\right)q_6^2\right] - g_{11}\left(P_1^2 \varepsilon_1 + P_2^2 \varepsilon_2 + P_3^2 \varepsilon_3\right) \\
&- g_{12}\left[\varepsilon_1\left(P_2^2 + P_3^2\right) + \varepsilon_2\left(P_1^2 + P_3^2\right) + \varepsilon_3\left(P_1^2 + P_2^2\right)\right] - g_{44}(P_1 P_2 \varepsilon_6 + P_1 P_3 \varepsilon_5 + P_2 P_3 \varepsilon_4) - \lambda_{11}\left(\varepsilon_1 q_1^2 + \varepsilon_2 q_2^2 + \varepsilon_3 q_3^2\right) \\
&- \lambda_{12}\left[\varepsilon_1\left(q_2^2 + q_3^2\right) + \varepsilon_2\left(q_3^2 + q_1^2\right) + \varepsilon_3\left(q_1^2 + q_2^2\right)\right] - \lambda_{44}(\varepsilon_4 q_2 q_3 + \varepsilon_5 q_3 q_1 + \varepsilon_6 q_1 q_2) - \varsigma_{11}\left(\varepsilon_1 q_4^2 + \varepsilon_2 q_5^2 + \varepsilon_3 q_6^2\right) \\
&- \varsigma_{12}\left[\varepsilon_1\left(q_5^2 + q_6^2\right) + \varepsilon_2\left(q_6^2 + q_4^2\right) + \varepsilon_3\left(q_4^2 + q_5^2\right)\right] - \varsigma_{44}(\varepsilon_4 q_5 q_6 + \varepsilon_5 q_6 q_4 + \varepsilon_6 q_4 q_5),
\end{aligned} \tag{7}
$$

where t_{ij}, κ_{ij}, g_{ij}, μ_{ij}, λ_{ij}, and ς_{ij} are coupling coefficients. The 33 parameters appearing in Table I were determined from a series of first-principles total-energy calculations on distorted perovskite structures.[21] Detailed information of the first-principles calculations and the approach to determining these coefficients can be found in Refs. 20 and 21. The parameters (in SI unit) converted from first-principles calculations are listed in the Table I.

TABLE I. The parameters converted from first-principles calculations[a] (Ref. 21; energy density unit: J/m^3).

α_1	-3.56×10^8
α_{11}	3.70×10^8
α_{12}	9.72×10^7
α_{111}	-1.18×10^7
α_{112}	-5.94×10^7
α_{122}	-2.68×10^8
β_1	-2.05×10^{29}
β_{11}	1.20×10^{49}
β_{12}	3.62×10^{48}
β_{111}	-2.89×10^{67}
β_{112}	-2.31×10^{68}
β_{122}	-4.92×10^{68}
γ_1	-1.85×10^{29}
$\gamma_{11} + \gamma_{12}$	1.48×10^{49}
$\gamma_{111} + \gamma_{112}$	-2.31×10^{68}
γ_{122}	
μ_{11}	-7.69×10^{49}
μ_{12}[b]	3.29×10^{48}
C_{11}	4.03×10^{11}
C_{12}	1.07×10^{11}
C_{44}	9.99×10^{10}
t_{11}	-1.53×10^{29}
t_{12}	-7.79×10^{28}
t_{44}	2.34×10^{29}
κ_{11}	-1.43×10^{29}
κ_{12}	-5.02×10^{28}
κ_{44}	
g_{11}	1.02×10^{10}
g_{12}	-1.76×10^9
g_{44}	7.70×10^9
λ_{11}	-2.10×10^{29}
λ_{12}	-9.85×10^{29}
λ_{44}	-1.24×10^{29}
ζ_{11}	0
ζ_{12}	-9.65×10^{29}
ζ_{44}	

[a]R_5^+ mode is neglected.
[b]Normalized by eliminating X_5^+ mode.

III. RESULTS AND DISCUSSION

A. AFD transitions

For the AFD transition with only one in-phase TiO$_6$ octahedron tilt and two out-of-phase TiO$_6$ octahedron tilts, i.e. $P_1 = P_2 = P_3 = q_3 = q_4 = q_5 = 0$, we have

$$
\begin{aligned}
F = &\ \beta_{10}\Theta_{S2}\left[\coth\left(\frac{\Theta_{S2}}{T}\right) - \coth\left(\frac{\Theta_{S2}}{T_2}\right)\right]\left(q_1^2 + q_2^2\right) \\
&+ \gamma_{10}\Theta_{S3}\left[\coth\left(\frac{\Theta_{S3}}{T}\right) - \coth\left(\frac{\Theta_{S3}}{T_3}\right)\right]q_6^2 \\
&+ \beta_{11}^*\left(q_1^2 + q_2^2\right)^2 + \beta_{12}^*\left(q_1^4 + q_2^4\right) + \beta_{111}\left(q_1^2 + q_2^2\right)^3 \\
&+ \beta_{112}\left(q_1^2 + q_2^2\right)\left(q_1^4 + q_2^4\right) + \left(\gamma_{11}^* + \gamma_{12}^*\right)q_6^4 \\
&+ \left(\gamma_{111} + \gamma_{112}\right)q_6^6 - \mu_{12}^*\left(q_1^2 + q_2^2\right)q_6^2,
\end{aligned} \tag{8}
$$

where β_{ij}^*, μ_{ij}^*, and γ_{ij}^* are normalized coefficients with stress-free boundary conditions (see Appendix for details). The order parameters and free energies of different structures are summarized in Table II.

According to experimental results, as discussed in the introduction, we can conclude that there are at least two AFD transitions, i.e. $Pm\bar{3}m$ to $I4/mcm$ and another transition to $Pbnm$. The latter cannot be a direct transition from $I4/mcm$ to $Pbnm$, if the energy of $Imma$ or $Cmcm$ is higher than $Pbnm$. As compared in Table II, appropriate selection of coefficients can generate different possibilities for the latter AFD transition sequence, such as $I4/mcm \rightarrow Imma \rightarrow Pbnm$, $I4/mcm \rightarrow Cmcm \rightarrow Pbnm$, etc. Carpenter[29] analyzed the energy difference between these structures and proposed an $I4/mcm \rightarrow Imma \rightarrow Pbnm$ transition sequence. It should be noted that the $Imma$ structure was not observed experimentally. Here, we propose another scenario for the transformation sequence, $I4/mcm \rightarrow Cmcm \rightarrow Pbnm$, although the existence of $Cmcm$ structure is still controversial in this system.[7,9–11] However, only this transition sequence can account for both the transition temperature of about 1380 K, which was determined by Guyot *et al.*[7] and Gillet *et al.*,[12] respectively, and Kennedy *et al.*'s neutron diffraction results.[9] According to Guyot *et al.*'s heat capacity measurement,[7] both $I4/mcm \rightarrow Cmcm$ and

TABLE II. The order parameters and free energies of different structures of AFD transitions.

Space group	Order parameters	Energy expression
$Pm\bar{3}m$	$q_i = 0, (i = 1, 2, 6)$	0
$I4/mcm$	$q_1 \neq 0$	$F_{I4/mcm} = \beta_1(T)q_1^2 + (\beta_{11}^* + \beta_{12}^*)q_1^4 + (\beta_{111} + \beta_{112})q_1^6$
$Imma$	$q_1 = q_2 \neq 0$	$F_{Imma} = 2\beta_1(T)q_1^2 + (4\beta_{11}^* + 2\beta_{12}^*)q_1^4 + (8\beta_{111} + 4\beta_{112})q_1^6$
$Cmcm$	$q_1 \neq q_6 \neq 0$	$F_{Cmcm} = \beta_1(T)q_1^2 + (\beta_{11}^* + \beta_{12}^*)q_1^4 + (\beta_{111} + \beta_{112})q_1^6 + \gamma_1(T)q_6^2$
$Cmcm$	$q_1 \neq q_6 \neq 0$	$+\gamma_1(T)q_6^2 + (\gamma_{11}^* + \gamma_{12}^*)q_6^4 + (\gamma_{111} + \gamma_{112})q_6^6 - \mu_{12}^*q_1^2q_6^2$
$Pbnm$	$q_1 = q_2 \neq 0, q_6 \neq 0$	$F_{Pbnm} = 2\beta_1(T)q_1^2 + (4\beta_{11}^* + 2\beta_{12}^*)q_1^4 + (8\beta_{111} + 4\beta_{112})q_1^6 + \gamma_1(T)q_6^2$
		$+(\gamma_{11}^* + \gamma_{12}^*)q_6^4 + (\gamma_{111} + \gamma_{112})q_6^6 - 2\mu_{12}^*q_1^2q_6^2$

$Cmcm \rightarrow Pbnm$ transitions are of the first order. For the $Pm\bar{3}m \rightarrow I4/mcm$ transition at about 1600 K, there is no or very small latent heat, which may be buried by the broad calorimetric peak of the previous transition.[7] Therefore, this transition may be of the second order or weakly first order. However, the tilt angles-vs-temperature diagram from the x-ray diffraction and neutron diffraction results[9,11] shows discontinuity near the transition temperature, a characteristic feature of a first-order transition.

In this paper, we adopted Guyot *et al.*'s[7] measured data of the transformation latent heat and assumed that the $Pm\bar{3}m \rightarrow I4/mcm$ transition is also of first order with a small latent heat of 1.0 kJ/mol. The saturation temperatures were estimated from the $(Ca,Sr)TiO_3$ phase diagrams.[30] The calculated values of β_{10} and γ_{10} by first principles show good agreement with the measured latent heat. So we simply adopted them to make the whole set of parameters consistent. The other parameters were determined by fitting Kennedy *et al.*'s[9] and Yashima *et al.*'s[11] neutron diffraction and x-ray diffraction data. A comparison between the fitted parameters and those from first principles is shown in Table III.

As shown in Table III, the fitted parameters deviate from those calculated by first principles. Both signs and magnitudes are different in almost every case. However, this can be expected because the first principles is for 0 K, and our fits are from the whole temperature range. The validity of the first-principles calculations can be tested by comparing the total free energy at 0 K from both sets of parameters. Actually, the difference is about 6.5% of the total free energy. Considering the possible errors and approximations made during the two calculations, this difference is small. In addition, the discrepancy is only confined to the parameters of the fourth- and sixth-order terms. The nice agreement between our fitted plot and the measured values (Fig. 2) indicates the accuracy of the parameters of the second-order terms and coupling terms from first principles. As shown in

Fig. 2, the fitted plot not only reproduces three first-order transitions but also shows the saturation of tilt angles at very low temperature. We also compared the free energy of these structures to study the phase stabilities, as plotted in Fig. 3. Although the differences between $I4/mcm$ and $Imma$ and between $Cmcm$ and $Pbnm$ are very small, the relative phase stability of different structures is just as we expected. And the small energy difference between $Cmcm$ and $Pbnm$ indicates the difficulty to get stable $Cmcm$ phase during *in-situ* x-ray diffraction and neutron diffraction experiments.

B. Ferroelectric transition

With the refined parameters, we can further investigate the AFD effect on ferroelectric transition in $CaTiO_3$ single crystals. Firstly, we can extract the Curie temperature T_1 from the extrapolated value (-111 K)[13] by eliminating the coupling effect from TiO_6 octahedron tilts. From our model, it is easy to calculate the T_1 for all the combinations of polarization in the three directions. And the calculated highest T_1 corresponds to the extrapolated ferroelectric effective temperature (-111 K).

By minimizing the free energy of the AFD part, we can calculate the in-phase tilt angle and out-of-phase angle as $\varphi_3 = 9.10°$ and $\theta_1 = \theta_2 = 8.64°$, respectively. Then using the tilt angles and the saturation temperature $\Theta_{S1} = 55$ K,[13] the T_1 of different polarization combinations are calculated. As listed in Table IV, the highest Curie temperature is 252.1 K for the case of $P_1 = P_2 \neq P_3$. This structure is therefore the most stable one, and this temperature is the Curie temperature T_1. Correspondingly, the parameter α_{10} is calculated as 1.77×10^6. So far, we have all the coefficients determined either from first-principles calculations or fitting from experimental data as summarized in Table V (in SI unit).

Because the tilt angles do not change much at low temperature, we can simply freeze them and calculate the

TABLE III. Parameters from fitting and their counterparts from first-principles calculations.

| Parameters	T_2 (K)	T_3 (K)	Θ_{S2} (K)	Θ_{S3} (K)	β_{10}	γ_1	β_{11}^*	β_{111}	β_{12}^*	β_{112}	$\gamma_{11}^* + \gamma_{12}^*$	$\gamma_{111} + \gamma_{112}$
From fitting	1285	1590	274	345			-1.41×10^{48}	1.45×10^{69}	-3.59×10^{48}	1.15×10^{69}	-3.38×10^{49}	1.15×10^{70}
From first principles					1.54×10^{26}	1.68×10^{26}	1.10×10^{49}	-2.89×10^{67}	2.64×10^{48}	-2.31×10^{68}	1.27×10^{49}	-2.31×10^{68}
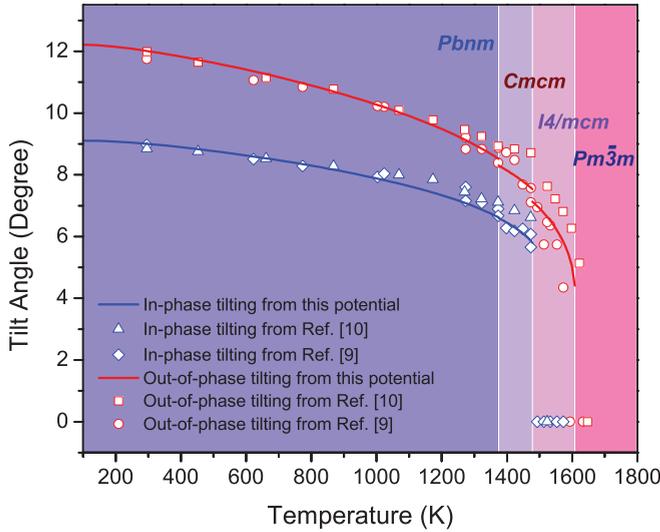
FIG. 2. (Color online) Tilt angle as a function of temperature. The discontinuities in the plot clearly show that there are three first-order transformations.

dielectric constant as a function of temperature. Thus, we get the coefficients of $P_1{}^2$ and $P_3{}^2$

$$\alpha_1^R = 2\alpha_{10}\Theta_{S1}\left[\coth\left(\frac{\Theta_{S1}}{T}\right) - \coth\left(\frac{\Theta_{S1}}{T_1}\right)\right]$$
$$- (2t_{11}^* + 2t_{12}^* + t_{44}^*)q_1^2 - 2\kappa_{12}^*q_6^2,$$
$$\alpha_3^R = \alpha_{10}\Theta_{S1}\left[\coth\left(\frac{\Theta_{S1}}{T}\right) - \coth\left(\frac{\Theta_{S1}}{T_1}\right)\right]$$
$$- (t_{11}^* + t_{12}^*)q_1^2 - 2\kappa_{11}^*q_6^2. \tag{9}$$

Experimentation shows that the intensity of the optical second harmonic generation (SHG) of $CaTiO_3$ thin film changes continuously as a function of temperature,[22] which
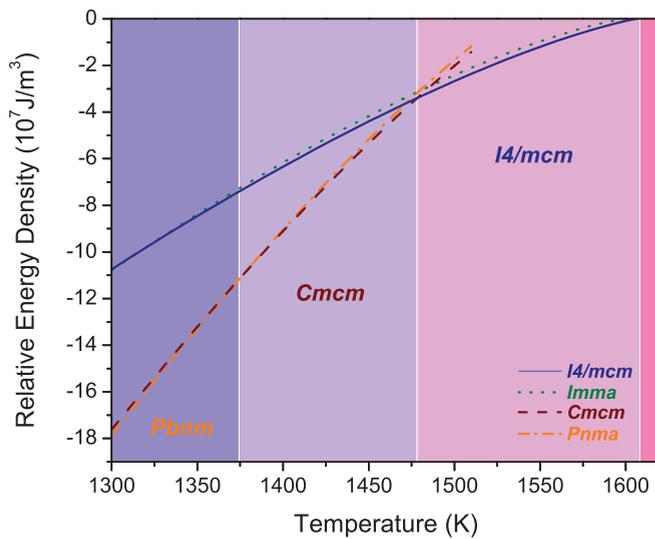
FIG. 3. (Color online) Relative free energy density of different structures: $I4/mcm$, $Imma$, $Cmcm$, and $Pbnm$. Note that $Pm\bar{3}m$ is set to be the reference state with free energy equal to zero. So the relative free energies of other structures are basically the energy difference from $Pm\bar{3}m$ structure.
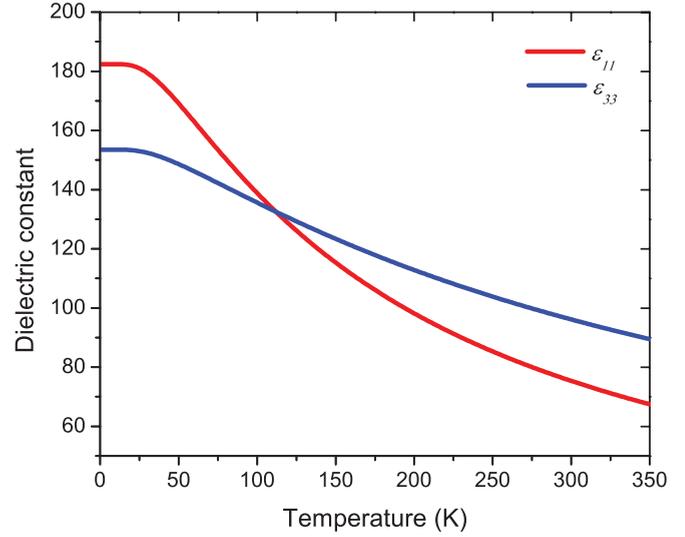
FIG. 4. (Color online) The dielectric constant as a function of temperature. The saturation of dielectric constants occurs at very low temperature.

indicates the ferroelectric transition of $CaTiO_3$ may be of the second order. However, the defects in the thin films, including strain inhomogeneity, domain structures, and so on, may make a first-order transformation look like a second-order one. Further studies are needed to understand the nature of ferroelectric transition in $CaTiO_3$. In this paper, we assume the ferroelectric transformation of $CaTiO_3$ is second order. According to Devonshire's theory,[1] the dielectric constant of a second-order transformation can be written as

$$\varepsilon_{ij} = \frac{1}{\varepsilon_0 \alpha_{ij}} \quad (i,j = 1,2,3), \tag{10}$$

where ε_0 is the vacuum permittivity, and α_{ij} is the coefficient of $P_i P_j$ $(i,j = 1,2,3)$. Since $P_1 = P_2$, it is easy to get $\varepsilon_{11} = \varepsilon_{22}$. The calculated dielectric constants are shown in Fig. 4. The total dielectric constant ($\sqrt{2\varepsilon_{11}^2 + \varepsilon_{33}^2}$) is 300 at 0 K, and 144 at room temperature. They are quite close to the measured values 331 and 168,[13] which indicate good accuracy for both the α_1 value from first-principles calculations and the Curie temperature T_1 from this calculation.

With all the temperature-dependent coefficients, we can investigate the phase stability under different boundary conditions. Here, we will calculate the temperature-constraint strain phase diagram of (001) $CaTiO_3$ thin film as an example.

For the stable structures of strained (001) $CaTiO_3$ thin films, Eklund et al.[20,21] reported two possible ferroelectric structures on the tensile strain side, $Pmc2_1$ and $Pmn2_1$, among which the $Pmn2_1$ structure has slightly lower free energy. Also from first-principles calculations, Bousquet[31] showed that $Pmc2_1$ is stable. On the compressive side, $Pna2_1$ is the stable structure.[21] In the following calculations, we will only consider these three structures.

Firstly, we renormalized the free energy expression with the thin film boundary condition (see Appendix for detail). By

TABLE IV. The calculated Curie temperatures for different polarization symmetry.

Polarization	$P_1 \neq P_2 \neq P_3$	$P_1 = P_2 \neq P_3$	$P_1 = -P_2 \neq P_3$	$P_1 = P_2 = P_3$
Curie temperature (K)	139.4	252.1	132.0	187.4

minimizing the total free energy with respect to q_1 and q_6, respectively, we get

$$\beta_1'(T) + (2\beta_{11}' + \beta_{12}')q_1^2 + 6(2\beta_{111} + \beta_{112})q_1^4 - \mu_{13}'q_6^2 = 0, \quad (11a)$$

$$\gamma_3'(T) + 2\gamma_{33}'q_6^2 + 3(\gamma_{111} + \gamma_{112})q_6^4 - 2\mu_{13}'q_1^2 = 0, \quad (11b)$$

TABLE V. The parameters for the phenomenological potential of CaTiO$_3$ from either first-principles calculations or experimental data (temperature unit: K, and energy density unit: J/m^3)

T_1	252.1
T_2	1589.7
T_3	1285.0
Θ_{S1}	55.0
Θ_{S2}	274.0
Θ_{S3}	345.0
α_{10}	1.77×10^6
α_{11}	3.70×10^8
α_{12}	9.72×10^7
α_{111}	-1.18×10^7
α_{112}	-5.94×10^7
α_{122}	-2.68×10^8
β_{10}	1.54×10^{26}
β_{11}	-4.28×10^{47}
β_{12}	-2.61×10^{48}
β_{111}	1.45×10^{69}
β_{112}	1.15×10^{69}
β_{122}	-4.92×10^{68}
γ_1	1.68×10^{26}
$\gamma_{11} + \gamma_{12}$	-3.17×10^{49}
$\gamma_{111} + \gamma_{112}$	1.15×10^{70}
γ_{122}	
μ_{11}	-7.69×10^{49}
μ_{12}	3.29×10^{48}
C_{11}	4.03×10^{11}
C_{12}	1.07×10^{11}
C_{44}	9.99×10^{10}
t_{11}	-1.53×10^{29}
t_{12}	-7.79×10^{28}
t_{44}	2.34×10^{29}
κ_{11}	-1.43×10^{29}
κ_{12}	-5.02×10^{28}
κ_{44}	
g_{11}	1.02×10^{10}
g_{12}	-1.76×10^9
g_{44}	7.70×10^9
λ_{11}	-2.10×10^{29}
λ_{12}	-9.85×10^{29}
λ_{44}	-1.24×10^{29}
ζ_{11}	0
ζ_{12}	-9.65×10^{29}
ζ_{44}	

where β_{ij}', μ_{ij}', and γ_{ij}' are normalized coefficients. Combining Eqs. (11a) and (11b) with the equation from the coefficient of P_1^2,

$$2\alpha_1'(T) - (2t_{11}' + 2t_{12}' + t_{44})q_1^2 - 2\kappa_{13}'q_6^2 = 0, \quad (12)$$

we can get the phase boundary between $Pbnm$ and $Pmc2_1$ structures. It should be mentioned here, from our potential, the stable structure on the tensile side is $Pmc2_1$, not $Pmn2_1$. Similarly, for the phase boundary of $Pbnm \rightarrow Pna2_1$ transition,


(a)

(b)
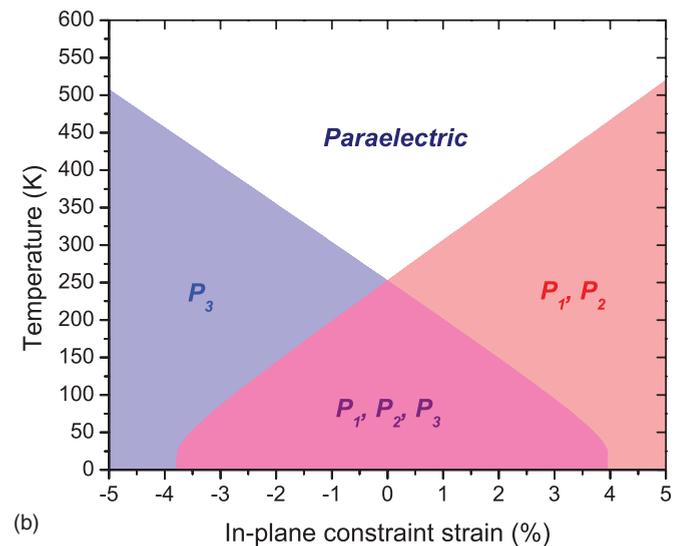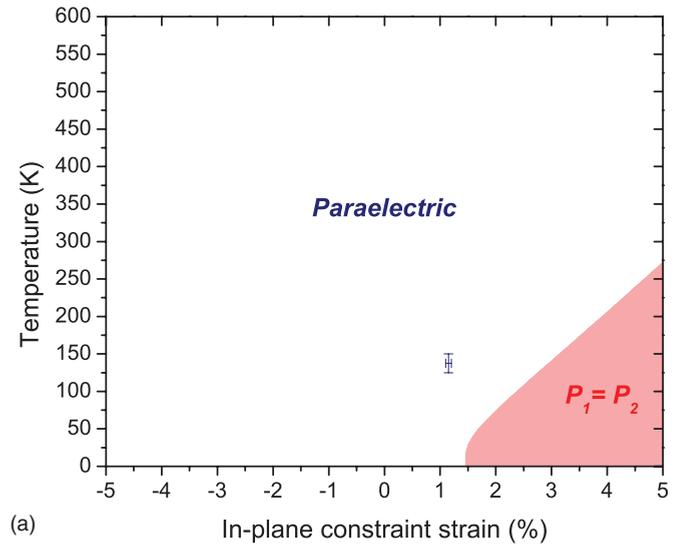
FIG. 5. (Color online) The temperature-constraint strain phase diagram of (001) CaTiO$_3$ (a) with AFD and (b) without AFD. The transition point shown in (a) is measured by SHG experiment.[22]
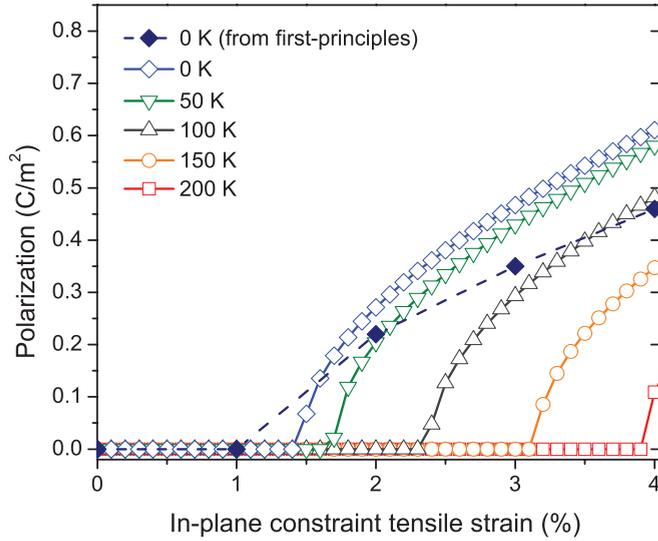
FIG. 6. (Color online) The polariztation of (001) CaTiO$_3$ thin film as a function of in-plain constraint strain of different temperatures. The void markers represent our calculations for different temperatures. And the solid diamonds denote the data from first-principles calculations (Ref. 21; solid diamond) for 0 K.

we need to solve Eqs. (11a) and (11b) and the equation from the coefficient of P_3^2,

$$2\alpha_3'(T) - 2t_{31}'q_1^2 - 2\kappa_{33}'q_6^2 = 0. \qquad (13)$$

The calculated phase diagram is asymmetric, as shown in Fig. 5(a). The minimum tensile strain to induce the ferroelectric transition is about 1.5%, which agrees well with the prediction from the first-principles calculations. On the compressive side of the diagram, about 13% compressive strain is needed to induce a $Pbnm \rightarrow Pna2_1$ transition. This value is so huge that it exceeds the limit of substrate constraint strain. In other words, it is impossible to have a $Pna2_1$ structure in (001) CaTiO$_3$ thin films. The temperature-constraint strain phase diagram of (001) CaTiO$_3$ thin film without AFD [Fig. 5(b)] was calculated by setting $q_i = 0$ ($i = 1$–6) and solving

$$\begin{vmatrix} \dfrac{\partial^2 F}{\partial P_1^2} & \dfrac{\partial^2 F}{\partial P_1 \partial P_2} & \dfrac{\partial^2 F}{\partial P_1 \partial P_3} \\[2mm] \dfrac{\partial^2 F}{\partial P_2 \partial P_1} & \dfrac{\partial^2 F}{\partial P_2^2} & \dfrac{\partial^2 F}{\partial P_2 \partial P_3} \\[2mm] \dfrac{\partial^2 F}{\partial P_3 \partial P_1} & \dfrac{\partial^2 F}{\partial P_3 \partial P_2} & \dfrac{\partial^2 F}{\partial P_3^2} \end{vmatrix}_{P_1 = P_2 = P_3 = 0} = 0. \qquad (14)$$

Comparing Figs. 5(a) and 5(b), we can easily find the asymmetry of the temperature-constraint strain phase diagram comes from the effect of AFD. Also the ferroelectric transition temperature of CaTiO$_3$ is greatly suppressed by AFD. A similar but weaker effect was also found in SrTiO$_3$.[32] The substantial effect of AFD on ferroelectricity in SrTiO$_3$ is attributed to the competitive anharmonic couplings between AFD mode and the ferroelectric mode and their mutual coupling to the elasticity.[2,16] In our phenomenological model of CaTiO$_3$, the stability of different structures is strongly dependent on the coupling coefficients among P_i, q_i, and ε_i, which can be easily seen from Eqs. (11a), (11b), (12), and (13).

This indicates that the competition mechanism between AFD and ferroelectricity is essentially the same as that of SrTiO$_3$.

By minimizing the total free energy, we also calculated the polarization of (001) CaTiO$_3$ thin film as a function of in-plane constraint tensile strain at different temperatures. As shown in Fig. 6, the ferroelectric transition temperature increases with in-plane tensile strain. At 0 K, the minimum tensile strain needed to induce the ferroelectric transition is about 1.5%. At 200 K, the critical tensile strain increases to about 4%, indicating the difficulty to obtain strain-induced ferroelectricity at elevated temperature. The calculated polarization of 4% tensile strain at 0 K is 0.61 C/m^2, which is more than twice that of BaTiO$_3$.[1] The polarization also exhibits saturation near the transition point and becomes linearly dependent on tensile strain in a large strain region. As compared in the figure, our result of 0 K is a little larger than the first-principles calculations. The discrepancy may rise from different selection of stable structures. In the first-principles calculation,[21] the stable structure used is $Pmc2_1$, whereas we computed the polarization of $Pmn2_1$.

IV. CONCLUSIONS

A phenomenological thermodynamic potential is developed for CaTiO$_3$ single crystals. The coefficients of the potential are determined from first-principles calculations and neutron diffraction and x-ray diffraction data. This potential effectively coupled the AFD transitions and strain-induced ferroelectric transitions. Several experimental observations, including transition temperatures, transition latent heat, dielectric constant, and tilt angles of TiO$_6$ octahedron, are successfully reproduced. Then the temperature-constraint strain single-domain phase diagram of (001) CaTiO$_3$ is constructed. The dependence of Curie temperature on constraint strain is quite asymmetric, i.e. only tensile strain can induce ferroelectric transition. Comparing the phase diagrams with and without AFD, we conclude that the asymmetry is not inherited from the ferroelectric transition itself but attributed from the AFD suppression.

APPENDIX

1. Relationship between order parameter q and octahedral tilt angles

For an infinitesimal angle, there is no octahedron distortion during tilting. In the 10-atom supercell, there are four atoms (all oxygen) that displace by equal amounts. The amplitude of $q_1 = 1$ means each atom moves 1 Å along x_1 direction. Then in a simplified diagram of TiO$_6$ octahedron tilt, we have

$$\tan\theta_i = \frac{2 \times (q_i \times 0.5)}{a_0} = \frac{q_i}{a_0} \quad (i = 1,2,3), \qquad (A1)$$

where θ_i is the in-phase tilt angle, and a_0 is the lattice parameter of the 5-atom cell. Similarly, we have the relationship for out-of-phase tilt

$$\tan \varphi_1 = \frac{q_i}{a_0} \quad (i = 4,5,6), \tag{A2}$$

where φ_i is the in-phase tilt angle.

2. Normalizing the total free energy with stress-free boundary condition

With the stress-free boundary condition, we have

$$\frac{\partial F}{\partial \varepsilon_{ij}} = \sigma_{ij} = 0. \tag{A3}$$

Then we can rewrite the expression for the total free energy as

$$
\begin{aligned}
F = {} & \alpha_{10}\Theta_{S1}\left[\coth\left(\frac{\Theta_{S1}}{T}\right) - \coth\left(\frac{\Theta_{S1}}{T_1}\right)\right](P_1^2 + P_2^2 + P_3^2) + \alpha_{11}^*(P_1^2 + P_2^2 + P_3^2)^2 + \alpha_{12}^*(P_1^4 + P_2^4 + P_3^4) \\
& + \alpha_{111}(P_1^2 + P_2^2 + P_3^2)^3 + \alpha_{112}(P_1^2 + P_2^2 + P_3^2)(P_1^4 + P_2^4 + P_3^4) + \alpha_{122}(P_1 P_2 P_3)^2 \\
& + \beta_{10}\Theta_{S2}\left[\coth\left(\frac{\Theta_{S2}}{T}\right) - \coth\left(\frac{\Theta_{S2}}{T_2}\right)\right](q_1^2 + q_2^2 + q_3^2) + \beta_{11}^*(q_1^2 + q_2^2 + q_3^2)^2 + \beta_{12}^*(q_1^4 + q_2^4 + q_3^4) \\
& + \beta_{111}(q_1^2 + q_2^2 + q_3^2)^3 + \beta_{112}(q_1^2 + q_2^2 + q_3^2)(q_1^4 + q_2^4 + q_3^4) + \beta_{122}(q_1 q_2 q_3)^2 \\
& + \gamma_{10}\Theta_{S3}\left[\coth\left(\frac{\Theta_{S3}}{T}\right) - \coth\left(\frac{\Theta_{S3}}{T_3}\right)\right](q_4^2 + q_5^2 + q_6^2) + \gamma_{11}^*(q_4^2 + q_5^2 + q_6^2)^2 + \gamma_{12}^*(q_4^4 + q_5^4 + q_6^4) \\
& + \gamma_{111}(q_4^2 + q_5^2 + q_6^2)^3 + \gamma_{112}(q_4^2 + q_5^2 + q_6^2)(q_4^4 + q_5^4 + q_6^4) + \gamma_{122}(q_4 q_5 q_6)^2 - \mu_{11}^*(q_1^2 q_4^2 + q_2^2 q_5^2 + q_3^2 q_6^2) \\
& - \mu_{12}^*\left[(q_2^2 + q_3^2)q_4^2 + (q_3^2 + q_1^2)q_5^2 + (q_1^2 + q_2^2)q_6^2\right] - t_{11}^*(P_1^2 q_1^2 + P_2^2 q_2^2 + P_3^2 q_3^2) \\
& - t_{12}^*\left[P_1^2(q_2^2 + q_3^2) + P_2^2(q_1^2 + q_3^2) + P_3^2(q_1^2 + q_2^2)\right] - t_{44}^*(P_1 P_2 q_1 q_2 + P_1 P_3 q_1 q_3 + P_2 P_3 q_2 q_3) \\
& - \kappa_{11}^*(P_1^2 q_4^2 + P_2^2 q_5^2 + P_3^2 q_6^2) - \kappa_{12}^*\left[P_1^2(q_5^2 + q_6^2) + P_2^2(q_4^2 + q_6^2) + P_3^2(q_4^2 + q_5^2)\right] \\
& - \kappa_{44}^*(P_1 P_2 q_4 q_5 + P_1 P_3 q_4 q_6 + P_2 P_3 q_5 q_6) - \frac{\zeta_{44}\lambda_{44}}{C_{44}}(q_2 q_3 q_5 q_6 + q_1 q_2 q_4 q_5 + q_1 q_3 q_4 q_6),
\end{aligned}
\tag{A4}
$$

where the * sign designates the renormalized coefficients, i.e.

$$
\begin{aligned}
\alpha_{11}^* &= \alpha_{11} - \frac{C_{11}(g_{12}^2 + 2g_{11}g_{12}) - C_{12}(g_{11}^2 + 2g_{12}^2)}{2(C_{11} - C_{12})(C_{11} + 2C_{12})} - \frac{g_{44}^2}{4C_{44}}, \quad \alpha_{12}^* = \alpha_{12} - \frac{(g_{11} - g_{12})^2}{2(C_{11} - C_{12})} + \frac{g_{44}^2}{4C_{44}}, \\
\beta_{11}^* &= \beta_{11} - \frac{C_{11}(\lambda_{12}^2 + 2\lambda_{11}\lambda_{12}) - C_{12}(\lambda_{11}^2 + 2\lambda_{12}^2)}{2(C_{11} - C_{12})(C_{11} + 2C_{12})} - \frac{\lambda_{44}^2}{4C_{44}}, \quad \beta_{12}^* = \beta_{12} - \frac{(\lambda_{11} - \lambda_{12})^2}{2(C_{11} - C_{12})} + \frac{\lambda_{44}^2}{4C_{44}}, \\
\gamma_{11}^* &= \gamma_{11} - \frac{C_{11}(\varsigma_{12}^2 + 2\varsigma_{11}\varsigma_{12}) - C_{12}(\varsigma_{11}^2 + 2\varsigma_{12}^2)}{2(C_{11} - C_{12})(C_{11} + 2C_{12})} - \frac{\varsigma_{44}^2}{4C_{44}}, \quad \gamma_{12}^* = \gamma_{12} - \frac{(\varsigma_{11} - \varsigma_{12})^2}{2(C_{11} - C_{12})} + \frac{\varsigma_{44}^2}{4C_{44}}, \\
\mu_{11}^* &= \mu_{11} + \frac{C_{11}(\lambda_{11}\varsigma_{11} + 2\lambda_{12}\varsigma_{12}) + C_{12}(\lambda_{11}\varsigma_{11} - 2\lambda_{11}\varsigma_{12} - 2\lambda_{12}\varsigma_{11})}{(C_{11} - C_{12})(C_{11} + 2C_{12})}, \\
\mu_{12}^* &= \mu_{12} - \frac{C_{12}(\lambda_{11}\varsigma_{11} + 2\lambda_{12}\varsigma_{12}) - C_{11}(\lambda_{12}\varsigma_{11} + \lambda_{11}\varsigma_{12} + \lambda_{12}\varsigma_{12})}{(C_{11} - C_{12})(C_{11} + 2C_{12})}. \\
t_{11}^* &= t_{11} + \frac{C_{11}(\lambda_{11}g_{11} + 2\lambda_{12}g_{12}) + C_{12}(\lambda_{11}g_{11} - 2\lambda_{11}g_{12} - 2\lambda_{12}g_{11})}{(C_{11} - C_{12})(C_{11} + 2C_{12})}, \\
t_{12}^* &= t_{12} - \frac{C_{12}(\lambda_{11}g_{11} + 2\lambda_{12}g_{12}) - C_{11}(\lambda_{12}g_{11} + \lambda_{11}g_{12} + \lambda_{12}g_{12})}{(C_{11} - C_{12})(C_{11} + 2C_{12})}, \\
t_{44}^* &= t_{44} + \frac{\lambda_{44}g_{44}}{C_{44}}, \quad \kappa_{11}^* = \kappa_{11} + \frac{C_{11}(\varsigma_{11}g_{11} + 2\varsigma_{12}g_{12}) + C_{12}(\varsigma_{11}g_{11} - 2\varsigma_{11}g_{12} - 2\varsigma_{12}g_{11})}{(C_{11} - C_{12})(C_{11} + 2C_{12})}, \\
\kappa_{12}^* &= \kappa_{12} - \frac{C_{12}(\varsigma_{11}g_{11} + 2\varsigma_{12}g_{12}) - C_{11}(\varsigma_{12}g_{11} + \varsigma_{11}g_{12} + \varsigma_{12}g_{12})}{(C_{11} - C_{12})(C_{11} + 2C_{12})}, \quad \kappa_{44}^* = \kappa_{44} + \frac{\varsigma_{44}g_{44}}{C_{44}}.
\end{aligned}
\tag{A5}
$$

3. Normalizing the total free energy with thin film boundary condition

The thin film boundary condition is a mixed set of strain and stress boundary conditions. For (001) CaTiO$_3$ thin film, there is a biaxial strain in the x_1-x_2 plane, and all the stress components associated with x_3 direction are equal to zero, i.e.

$$\varepsilon_{11} = \varepsilon_{22} = \varepsilon_S, \quad \varepsilon_{12} = \varepsilon_{21} = 0,$$
$$\sigma_{13} = \sigma_{23} = \sigma_{31} = \sigma_{32} = \sigma_{33} = 0,$$

(A6)

where ε_S is the constraint strain. To satisfy the above stress-free condition it requires that

$$\frac{\partial F}{\partial \varepsilon_{ij}} = \sigma_{ij} = 0 \quad (ij = 13,23,31,32,33).$$

(A7)

So we have

$$
\begin{aligned}
F = {} & \alpha_1'(T)\big(P_1^2 + P_2^2\big) + \alpha_3'(T)P_3^2 + \alpha_{11}'\big(P_1^4 + P_2^4\big) + \alpha_{33}'P_3^4 + \alpha_{12}'P_1^2 P_2^2 + \alpha_{13}'\big(P_1^2 + P_2^2\big)P_3^2 + \alpha_{111}\big(P_1^2 + P_2^2 + P_3^2\big)^3 \\
& + \alpha_{112}\big(P_1^2 + P_2^2 + P_3^2\big)\big(P_1^4 + P_2^4 + P_3^4\big) + \alpha_{122}(P_1 P_2 P_3)^2 + \beta_1'(T)\big(q_1^2 + q_2^2\big) + \beta_3'(T)q_3^2 + \beta_{11}'\big(q_1^4 + q_2^4\big) + \beta_{33}'q_3^4 \\
& + \beta_{12}'q_1^2 q_2^2 + \beta_{13}'\big(q_1^2 + q_2^2\big)q_3^2 + \beta_{111}\big(q_1^2 + q_2^2 + q_3^2\big)^3 + \beta_{112}\big(q_1^2 + q_2^2 + q_3^2\big)\big(q_1^4 + q_2^4 + q_3^4\big) + \beta_{122}(q_1 q_2 q_3)^2 \\
& + \gamma_1'(T)\big(q_4^2 + q_5^2\big) + \gamma_3'(T)q_6^2 + \gamma_{11}'\big(q_4^4 + q_5^4\big) + \gamma_{33}'q_6^4 + \gamma_{12}'q_4^2 q_5^2 + \gamma_{13}'\big(q_4^2 + q_5^2\big)q_6^2 + \gamma_{111}\big(q_4^2 + q_5^2 + q_6^2\big)^3 \\
& + \gamma_{112}\big(q_4^2 + q_5^2 + q_6^2\big)\big(q_4^4 + q_5^4 + q_6^4\big) + \gamma_{122}(q_4 q_5 q_6)^2 - \mu_{11}'\big(q_1^2 q_4^2 + q_2^2 q_5^2\big) - \mu_{33}'q_3^2 q_6^2 - \mu_{12}'\big(q_2^2 q_4^2 + q_1^2 q_5^2\big) \\
& - \mu_{13}'\big(q_1^2 + q_2^2\big)q_6^2 - \mu_{31}'\big(q_4^2 + q_5^2\big)q_3^2 - t_{11}'\big(P_1^2 q_1^2 + P_2^2 q_2^2\big) - t_{33}'P_3^2 q_3^2 - t_{12}'\big(P_1^2 q_2^2 + P_2^2 q_1^2\big) - t_{13}'\big(P_1^2 + P_2^2\big)q_3^2 \\
& - t_{31}'\big(q_1^2 + q_2^2\big)P_3^2 - t_{44}P_1 P_2 q_1 q_2 - t_{44}'(P_1 P_3 q_1 q_3 + P_2 P_3 q_2 q_3) - \kappa_{11}'\big(P_1^2 q_4^2 + P_2^2 q_5^2\big) - \kappa_{33}'P_3^2 q_6^2 - \kappa_{12}'\big(P_1^2 q_5^2 + P_2^2 q_4^2\big) \\
& - \kappa_{13}'\big(P_1^2 + P_2^2\big)q_6^2 - \kappa_{31}'\big(q_4^2 + q_5^2\big)P_3^2 - \kappa_{44}P_1 P_2 q_4 q_5 - \kappa_{44}'(P_1 P_3 q_4 q_6 + P_2 P_3 q_5 q_6) - \frac{\zeta_{44}\lambda_{44}}{C_{44}}(q_2 q_3 q_5 q_6 + q_1 q_3 q_4 q_6) \\
& + \frac{(C_{11} + 2C_{12})(C_{11} - C_{12})}{C_{11}}\varepsilon_S^2,
\end{aligned}
$$

(A8)

where the $'$ sign represents the renormalized coefficients with thin film boundary condition, i.e.

$$\alpha_1'(T) = \alpha_1(T) - \left(g_{11} + g_{12} - \frac{2C_{12}}{C_{11}}g_{12}\right)\varepsilon_S, \quad \alpha_3'(T) = \alpha_1(T) - \left(2g_{12} - \frac{2C_{12}}{C_{11}}g_{11}\right)\varepsilon_S, \quad \alpha_{11}' = \alpha_{11} + \alpha_{12} - \frac{g_{12}^2}{2C_{11}},$$

$$\alpha_{33}' = \alpha_{11} + \alpha_{12} - \frac{g_{11}^2}{2C_{11}}, \quad \alpha_{12}' = 2\alpha_{11} - \frac{g_{12}^2}{C_{11}}, \quad \alpha_{13}' = 2\alpha_{11} - \left(\frac{g_{11}g_{12}}{C_{11}} + \frac{g_{44}^2}{2C_{44}}\right),$$

$$\beta_1'(T) = \beta_1(T) - \left(\lambda_{11} + \lambda_{12} - \frac{2C_{12}}{C_{11}}\lambda_{12}\right)\varepsilon_S, \quad \beta_3'(T) = \beta_1(T) - \left(2\lambda_{12} - \frac{2C_{12}}{C_{11}}\lambda_{11}\right)\varepsilon_S, \quad \beta_{11}' = \beta_{11} + \beta_{12} - \frac{\lambda_{12}^2}{2C_{11}},$$

$$\beta_{33}' = \beta_{11} + \beta_{12} - \frac{\lambda_{11}^2}{2C_{11}}, \quad \beta_{12}' = 2\beta_{11} - \frac{\lambda_{12}^2}{C_{11}}, \quad \beta_{13}' = 2\beta_{11} - \left(\frac{\lambda_{11}\lambda_{12}}{C_{11}} + \frac{\lambda_{44}^2}{2C_{44}}\right),$$

$$\gamma_1'(T) = \gamma_1(T) - \left(\varsigma_{11} + \varsigma_{12} - \frac{2C_{12}}{C_{11}}\varsigma_{12}\right)\varepsilon_S, \quad \gamma_3'(T) = \gamma_1(T) - \left(2\varsigma_{12} - \frac{2C_{12}}{C_{11}}\varsigma_{11}\right)\varepsilon_S, \quad \gamma_{11}' = \gamma_{11} + \gamma_{12} - \frac{\varsigma_{12}^2}{2C_{11}},$$

$$\gamma_{33}' = \gamma_{11} + \gamma_{12} - \frac{\varsigma_{11}^2}{2C_{11}}, \quad \gamma_{12}' = \left(2\gamma_{11} - \frac{\varsigma_{12}^2}{C_{11}}\right), \quad \gamma_{13}' = 2\gamma_{11} - \left(\frac{\varsigma_{11}\varsigma_{12}}{C_{11}} + \frac{\varsigma_{44}^2}{2C_{44}}\right),$$

$$\mu_{11}' = \mu_{11} + \frac{\varsigma_{12}\lambda_{12}}{C_{11}}, \quad \mu_{33}' = \mu_{11} + \frac{\varsigma_{11}\lambda_{11}}{C_{11}}, \quad \mu_{12}' = \mu_{12} + \frac{\varsigma_{12}\lambda_{12}}{C_{11}}, \quad \mu_{13}' = \mu_{12} + \frac{\varsigma_{11}\lambda_{12}}{C_{11}}, \quad \mu_{31}' = \mu_{12} + \frac{\varsigma_{12}\lambda_{11}}{C_{11}},$$

$$t_{11}' = t_{11} + \frac{g_{12}\lambda_{12}}{C_{11}}, \quad t_{33}' = t_{11} + \frac{g_{11}\lambda_{11}}{C_{11}}, \quad t_{12}' = t_{12} + \frac{g_{12}\lambda_{12}}{C_{11}}, \quad t_{13}' = t_{12} + \frac{g_{12}\lambda_{11}}{C_{11}},$$

$$t_{31}' = t_{12} + \frac{g_{11}\lambda_{12}}{C_{11}}, \quad t_{44}' = t_{44} + \frac{g_{44}\lambda_{44}}{C_{44}},$$

$$\kappa_{11}' = \kappa_{11} + \frac{g_{12}\varsigma_{12}}{C_{11}}, \quad \kappa_{33}' = \kappa_{11} + \frac{g_{11}\varsigma_{11}}{C_{11}}, \quad \kappa_{12}' = \kappa_{12} + \frac{\varsigma_{12}g_{12}}{C_{11}}, \quad \kappa_{13}' = \kappa_{12} + \frac{\varsigma_{11}g_{12}}{C_{11}},$$

$$\kappa_{31}' = \kappa_{12} + \frac{\varsigma_{12}g_{11}}{C_{11}}, \quad \kappa_{44}' = \kappa_{44} + \frac{\varsigma_{44}g_{44}}{C_{44}}.$$

(A9)

*Corresponding author: Yijia Gu, N-324 Millennium Science Complex, University Park, PA 16802; yug115@psu.edu

[1] M. E. Lines and A. M. Glass, *Principles and Applications of Ferroelectrics and Related Materials*, 1st ed. (Oxford University Press, Oxford, 1977).

[2] W. Zhong and D. Vanderbilt, Phys. Rev. Lett. **74**, 2587 (1995).

[3] D. Vanderbilt and W. Zhong, Ferroelectrics **206**, 181 (1998).

[4] J. H. Haeni, P. Irvin, W. Chang, R. Uecker, P. Reiche, Y. L. Li, S. Choudhury, W. Tian, M. E. Hawley, B. Craigo, A. K. Tagantsev, X. Q. Pan, S. K. Streiffer, L. Q. Chen, S. W. Kirchoefer, J. Levy, and D. G. Schlom, Nature **430**, 758 (2004).

[5] A. M. Glazer, Acta Crystallogr. Sect. B **28**, 3384 (1972).

[6] P. Gillet, F. Guyot, G. D. Price, B. Tournerie, and A. Lecleach, Phys. Chem. Miner. **20**, 159 (1993).

[7] F. Guyot, P. Richet, P. Courtial, and P. Gillet, Phys. Chem. Miner. **20**, 141 (1993).

[8] S. A. T. Redfern, J. Phys. Condens. Matter **8**, 8267 (1996).

[9] B. J. Kennedy, C. J. Howard, and B. C. Chakoumakos, J. Phys. Condens. Matter **11**, 1479 (1999).

[10] R. Ali and M. Yashima, J. Solid State Chem. **178**, 2867 (2005).

[11] M. Yashima and R. Ali, Solid State Ionics **180**, 120 (2009).

[12] P. Gillet, G. Fiquet, I. Daniel, and B. Reynard, Geophys. Res. Lett. **20**, 1931 (1993).

[13] V. V. Lemanov, A. V. Sotnikov, E. P. Smirnova, M. Weihnacht, and R. Kunze, Solid State Commun. **110**, 611 (1999).

[14] E. Cockayne and B. P. Burton, Phys. Rev. B **62**, 3735 (2000).

[15] V. Zelezny, E. Cockayne, J. Petzelt, M. F. Limonov, D. E. Usvyat, V. V. Lemanov, and A. A. Volkov, Phys. Rev. B **66**, 224303 (2002).

[16] N. Sai and D. Vanderbilt, Phys. Rev. B **62**, 13942 (2000).

[17] S. Bhattacharjee, E. Bousquet, and P. Ghosez, Phys. Rev. Lett. **102**, 117602 (2009).

[18] S. Amisi, E. Bousquet, K. Katcho, and Ph. Ghoset, Phys. Rev. B **85**, 064112 (2012).

[19] James M. Rondinelli and Craig J. Fennie, e-print arXiv:1106.0049 (to be published).

[20] C. J. Eklund, C. J. Fennie, and K. M. Rabe, Phys. Rev. B **79**, 220101 (2009).

[21] C. J. Eklund, Ph.D. thesis, Rutgers University, 2010.

[22] E. Vlahos, Ph.D. thesis, Pennsylvania State University, 2011.

[23] M. Calleja, M. T. Dove, and E. K. H. Salje, J. Phys. Condens. Matter **15**, 2301 (2003).

[24] L. Goncalves-Ferreira, S. A. T. Redfern, E. Artacho, E. Salje, and W. T. Lee, Phys. Rev. B **81**, 024109 (2010).

[25] W. T. Lee, E. K. H. Salje, L. Goncalves-Ferreira, M. Daraktchiev, and U. Bismayer, Phys. Rev. B **73**, 214110 (2006).

[26] L. Goncalves-Ferreira, S. A. T. Redfern, E. Atacho, and E. K. H. Salje, Appl. Phys. Lett. **94**, 081903 (2009).

[27] L. Goncalves-Ferreira, S. A. T. Redfern, E. Artacho, and E. K. H. Salje, Phys. Rev. Lett. **101**, 097602 (2008).

[28] M. A. Carpenter, A. I. Becerro, and F. Seifert, Am. Mineral. **86**, 348 (2001).

[29] M. A. Carpenter, Am. Mineral. **92**, 309 (2007).

[30] M. A. Carpenter, C. J. Howard, K. S. Knight, and Z. Zhang, J. Phys. Condens. Matter **18**, 10725 (2006).

[31] E. Bousquet (unpublished data).

[32] Y. L. Li, S. Choudhury, J. H. Haeni, M. D. Biegalski, A. Vasudevarao, A. Sharan, H. Z. Ma, J. Levy, V. Gopalan, S. Trolier-McKinstry, D. G. Schlom, Q. X. Jia, and L. Q. Chen, Phys. Rev. B **73**, 184112 (2006).